

# Split boss diaphragm based fiber Bragg grating pressure sensor with increased sensitivity

MANJUNATH MANUVINAKURAKE<sup>a,\*</sup>, UMA GANDHI<sup>c</sup>, UMAPATHY MANGALANATHAN<sup>c</sup>,  
SUNEETHA SEBASTIAN<sup>b</sup>, ASOKAN SUNDARRAJAN<sup>b</sup>, DHANANJAY YADAV<sup>a</sup>, MANJUNATHA NAYAK<sup>a</sup>

<sup>a</sup>Centre for Nano Science and Engineering, Indian Institute of Science, Bangalore, 560012, India

<sup>b</sup>Department of Instrumentation and Applied Physics, Indian Institute of Science, Bangalore, 560012, India

<sup>c</sup>Department of Instrumentation and Control Engineering, National Institute of Technology, Tiruchirappalli, 620015, India

In the proposed work we would like to present a stainless steel (SS) based pressure sensor using a split boss diaphragm mounted with a fiber Bragg grating (FBG) at its centre. This proposed stress transfer mechanism provides maximum stress to the fiber, resulting in improved sensitivity. The sensor is fabricated and tested for its performance for both static as well as dynamic pressure and is also benchmarked with a flat diaphragm pressure sensor. The developed sensor exhibits an enhanced pressure sensitivity of 0.742 nm/bar, which is ~10 times higher than the flat diaphragm based sensor. The sensor's dynamic sensing characteristics of peak output, rise time were 4.94 nm and 1.2 ms respectively.

(Received January 20, 2020; accepted April 8, 2021)

**Keywords:** Pressure sensor, Flat diaphragm, Split boss diaphragm, Fiber Bragg grating

## 1. Introduction

The key structural component of any pressure sensor is a thin circular or square diaphragm which deforms under applied pressure. Secondary sensing elements such as thin film strain gauges, diffused resistors, FBG's *etc* which are embedded in the highly stressed regions of the diaphragm, convert the stress on the diaphragm, induced due to input pressure, into an electrical or optical output. By modifying dimensions of the structure and the structure itself, a wide range of pressure measurement can be accomplished. Thereby in developing pressure sensors with high sensitivity and linearity, structures play a very important role, as they undergo deformation to the input pressure and function as the primary sensing element of the sensor.

Hence considerable attention is given to the development of innovative structures. To achieve high sensitivity, thinner diaphragms are required, however excessively thin diaphragms may induce large deflection and instability, thus leading to the unfavorable performances of a sensor in terms of linearity and repeatability. Therefore, design and optimization of various geometrical parameters of the structure are very critical.

Substantial progress in sensing characteristics have been achieved by using structures such as Bourdon tubes [1], bellows [2,3], cylindrical shells [4], varied forms of diaphragms [5-9], beams [10] as well combination of diaphragms and beams [11,12], as they play a key role in transmitting stress to the secondary sensing elements. Varied materials have been used to fabricate these primary structural elements of the sensor, such as stainless steel [5,6,8], elastomers [13], polymers [14,15] *etc*. Metallic

diaphragms due to their superior elastic characteristics and their compatibility for use in corrosive and high pressure environments have found wide spread usage.

Wide array of secondary sensing techniques, like fiber optic based sensing by Yan Sun *et.al.* [8], piezoresistive by Vinoth Kumar *et.al.*[16], piezoelectric by Sujan Y *et.al.* [17], and capacitive by Giulio Fragiaco *et.al.* [18] have been used in conjunction with the primary sensing element, to improve upon the sensitivity and other key characteristics of pressure sensors. In this work fiber optic based, Fiber Bragg grating (FBG) strain sensors has been taken up for study as they offer significant advantages over conventional sensors, such as high sensitivity, fast response, small foot print, easy fabrication, chemical inertness, and immunity to Electromagnetic Interference (EMI) as highlighted by Raman Kashyap [19]. It works on the principal of change in Bragg wavelength due to strain, resulting due to applied pressure. Different types of FBG based sensors have been developed to measure various measurands, such as temperature [20], strain [21], level [22], flow [23], displacement [24], pressure [5,6,11,12,] *etc*, either by manipulating effective refractive index or the grating period of FBG. By designing appropriate primary sensing mechanical systems in conjunction with the secondary sensing element, highly sensitive sensors with desired attributes for many given applications can be achieved. Varied schemes of aligning FBGs on to the structural element of pressure sensor have been employed, to improve the performance of sensors. A pressure sensor with two FBG's bonded on to the SS circular diaphragm, with one adjacent to the edge of diaphragm to detect negative strain, while another FBG fixed to the center of diaphragm to detect positive strain, developed and tested by Jun H. and Zude Z. [5] showed a

sensitivity, linearity of 1.57 pm/kPa and 99.996%, another pressure sensor by Vengal R. *et.al.* [2] with a single FBG attached along the central axis of metal bellows has showed a sensitivity, linearity of 90.6 pm/psi and 99.86%. Yet another sensor with a single strand FBG bonded along its central axis to the circular diaphragm designed by Yanling Xiong *et.al.* [25] showed a sensitivity and linearity of 0.023nm/MPa and 97.20%. Pressure sensors with diaphragm-cantilever structure, consisting of a flat circular metal diaphragm, connected to a cantilever with two FBG's bonded on to the top and bottom of cantilever by Yong Zhao *et.al.*[26], displayed a sensitivity, linearity of 258.28 pm/MPa and 99.99%. Another unique pressure sensor consisting of a SS diaphragm coupled to a fixed guided beam with two FBGs bonded in the tensile and compressive regions of the beam developed and tested by Manjunath. M *et.al.* [11] has displayed a sensitivity and linearity of 0.103 nm/bar and 99.94% respectively.

All the above study suggests that to achieve higher sensitivity and linearity, novel ways of designing the primary sensing element, along with alignment of FBG is very much crucial.

This paper presents a compact stainless steel based split boss diaphragm pressure sensor, consisting of a circular diaphragm and a split rigid circular mass referred to as split boss at its centre. A FBG is bonded at the centre, bridging the two halves of split boss, to capture strain induced due to applied pressure. The benefit of the planned sensor is that it is fabricated as a single integrated entity and the stress transmitting mechanism projected, provides maximum strain onto the FBG.

The proposed sensor exhibits improved sensitivity with good linearity and repeatability for a pressure range of 0-8 bar. The use of stainless steel metal diaphragm enables the sensor for higher pressure range and corrosive environments, compared to the already accounted sensors in the literature survey.

## 2. Sensor design and principle

The 3D and cross sectional view of the planned sensor is shown in Fig. 1. It consists of a split boss diaphragm made of stainless steel (SS) as the primary sensing element and a FBG strain sensor, bonded across the centre of split boss as secondary sensing element. The primary sensing element as shown in Fig. 2a consists of a circular diaphragm of radius  $a$ , thickness  $h$ , along with a circular rigid mass which is split at its centre referred to as split boss, of radius  $b$ , split distance  $c$ , and height  $i$ . This primary sensing mechanical structure is later laser welded on to a SS adapter with M14 x 1.5 thread as shown in Fig. 1a, for applying pressure  $P$ . The fabricated FBG fiber sensing element of diameter  $d_f$ , length  $l_f$  and period  $\Lambda$ , is bonded across the centre of split boss to complete the assembly process of the sensor. The completely integrated sensor is as shown in Fig. 1c.

When pressure  $P$  is applied on to the diaphragm through the adapter, the split boss gets pulled apart, causing tensile strain on the fiber optic sensor. By determining strain on the fiber, applied pressure can be determined, as strain on the fiber is directly proportional to applied pressure. The forces and moments acting on one half of the split boss are as shown in Fig.2c where  $M_f$  is the moment due to the fiber,  $M_{pr}$  moment due to the applied pressure and  $M_{sh}$  moment due to the shear force  $Q$  per unit length, with moments taken by the reference point A in the radial  $x$ - $y$  plane. The moment on the fiber  $M_f$  due to the deflection, of split boss is given by [27],

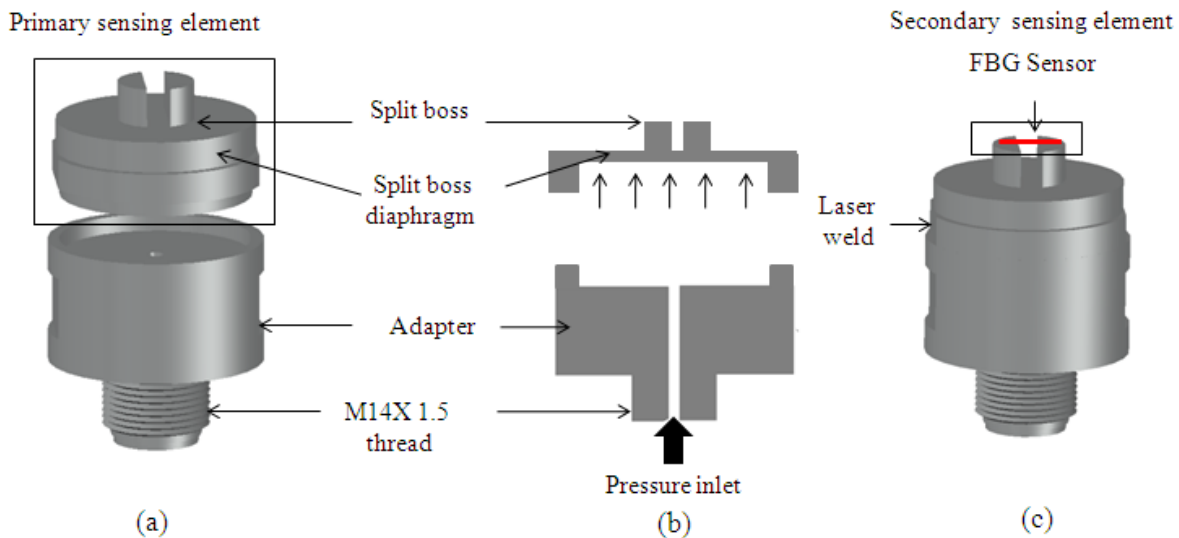


Fig. 1. 3D and cross sectional view of assembled sensor. (a) Primary sensing element and adapter for pressurizing (b) Sectional view of the primary sensing element and the adapter and (c) Complete sensor assembly

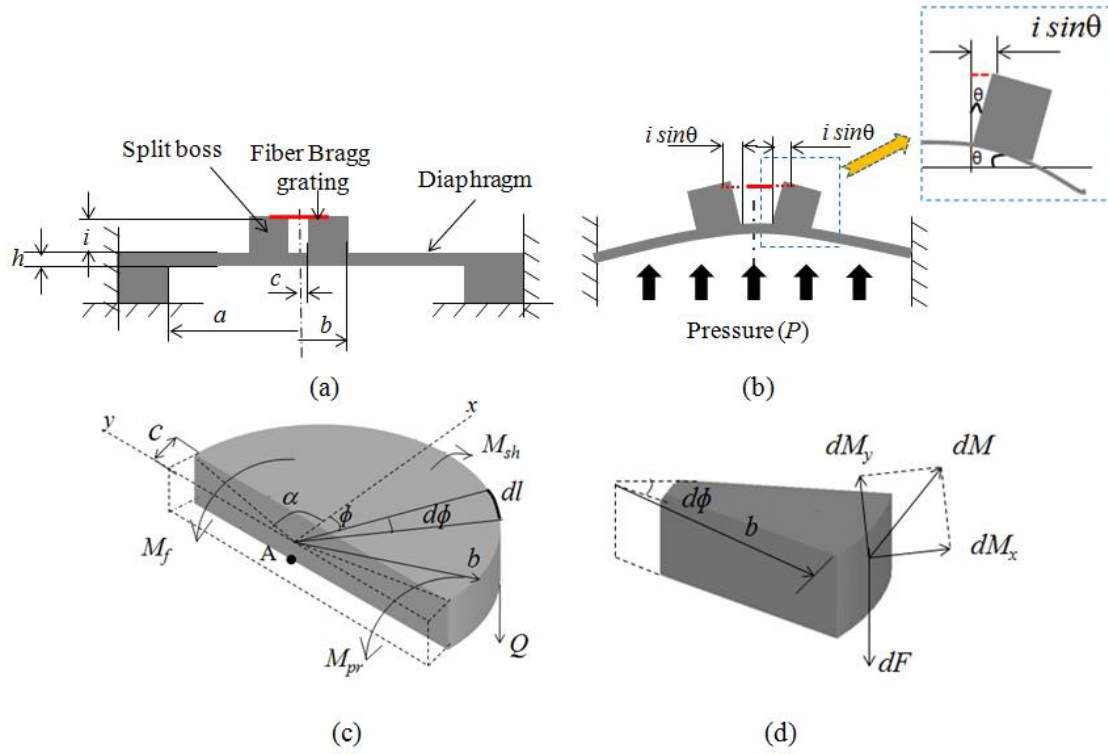


Fig. 2. Cross sectional images of the sensor. (a) Sectional view of split boss diaphragm without pressure (b) Sectional view of split boss diaphragm under pressure. (c) One half of split boss representing various moments and dimensions. (d) Section of the split boss (color online)

$$M_f = \text{Force} \times \text{distance} = \frac{2E_f A_f}{l_f} i \sin \theta i \cos \theta = \frac{E_f A_f i^2}{l_f} \sin 2\theta \quad (1)$$

where  $A_f$ ,  $E_f$  and  $\theta$  are the area, young's modulus of the fiber and angle subtended by the split boss due to the applied pressure.

The moment due to applied pressure  $M_{pr}$  is given by,

$$M_{pr} = \text{pressure} \times \text{area} \times \text{dis} \tan ce = P \left( \frac{\pi b^2}{2} - 2bc \right) (r_c - c) \quad (2)$$

where  $r_c$  is the distance of centroid of the circular segment from the centre [28]

$$r_c = \frac{4b \sin^3(\alpha)}{3(2\alpha - \sin(2\alpha))} \quad (3)$$

The angle  $\alpha$  of the circular segment which is part of split boss is given by

$$\sin(90 - \alpha) = \frac{c}{b} = \cos \alpha \quad \alpha = \cos^{-1} \frac{c}{b} \quad (4)$$

The shear force  $Q$  on the split boss per unit length is given by

$$Q \times \text{circumference} = \text{pressure} \times \text{area}$$

$$Q * \pi b = P \left( \frac{\pi b^2}{2} \right) \quad (5)$$

$$Q = \frac{Pb}{2} \quad (6)$$

Considering a section of the split boss, subtending an angle  $d\phi$ , and its outer edge length  $dl$ , representing the force  $dF$  and the moments in radial  $x$ - $y$  plane as shown in Fig. 2d.

The outer edge length  $dl$  will thereby be represented as

$$dl = b d\phi \quad (7)$$

The force on the edge length  $dl$  will be

$$dF = Q dl = Q b d\phi \quad (8)$$

As the moments are dispersed all along the edges of split boss, summing up the moments  $\vec{dM}$  will result in cancellation of the  $x$  components and summation of the  $y$  components thereby,

$$M_y = b \cos \phi dF = Q b^2 \cos \phi d\phi \quad (9)$$

The moment induced due to the shear force within the limits of  $-\alpha$  to  $\alpha$ , of the split boss will thereby be,

$$M_{sh} = \int_{-\alpha}^{\alpha} Qb^2 \cos \phi d\phi = Qb^2 \int_{-\alpha}^{\alpha} \cos \phi d\phi = Qb^2 [\sin \phi]_{-\alpha}^{\alpha} = 2Qb^2 \sin \alpha \quad (10)$$

For equilibrium of moments in the radial  $x$ - $y$  plane, with moments taken at reference point A,

$$M_{sh} = M_{pr} + M_f \quad (11)$$

thereby from equations (1, 2 and 10)

$$2Qb^2 \sin \alpha = P \left( \frac{\pi b^2}{2} - 2bc \right) (r_c - c) + \frac{E_f A_f i^2}{l_f} \sin 2\theta \quad (12)$$

The angle subtended by the split boss will be

$$2\theta = \sin^{-1} \left( \frac{(M_{sh} - M_{pr}) l_f}{E_f A_f i^2} \right) \quad (13)$$

Thereby the strain  $\varepsilon_f$  on the fiber is given by

$$\varepsilon_f = \frac{2 \times i \times \sin \theta}{l_f} \quad (14)$$

This strain is captured by the FBG which is reflected by shift in Bragg wavelength, where the relative shift in Bragg wavelength is given by [19, 29,30]

$$\frac{\Delta \lambda_b}{\lambda_b} = [(1 - p_e) \Delta \varepsilon_f] \quad (15)$$

$p_e$  is the effective photoelastic coefficient constant and  $\Delta \varepsilon_f$  is the change in strain due to applied pressure.

The reflected Bragg wavelength ( $\lambda_b$ ) is given by

$$\lambda_b = 2\eta \Lambda \quad (16)$$

where  $\eta$  and  $\Lambda$  are the refractive index and pitch of the grating of the fiber.

The relative shift in Bragg wavelength, experienced by fiber Bragg grating, due to strain, induced by the application of input pressure, on to the sensor is thereby given by

$$\frac{\Delta \lambda_b}{\lambda_b} = (1 - p_e) \frac{2 \times i \times \sin \theta}{l_f} \quad (17)$$

The change in Bragg wavelength, is dynamically logged by a FBG interrogator system. By interrogating the

shift in Bragg wavelength, the input pressure can be quantified.

The strain ( $\varepsilon$ ) on the fiber which is an important sensor characteristic is also benchmarked using three methodologies namely analytical, numerical simulation and then confirmed experimentally.

### 3. Sensor fabrication and testing

The schematic diagram of split boss structure FBG pressure sensor is as depicted in Fig. 1. It is made up of two critical elements, first being the primary sensing element which is the split boss structure consisting of a circular diaphragm and a circular boss split at its centre. This structure is laser welded on to the pressure port which has an integrated M14X1.5 thread connector used for applying pressure. This complete structure is fabricated using 17-4 Ph steel, known for its good corrosion resistance, which is a very much desirable property for a pressure sensor, as they can be used in corrosive environments. Well known machining processes such as CNC (Computer numerical control) turning, boring along with wire EDM process have been adopted to realize the primary sensing element structure with the parameters used in the pressure sensor design is as given in Table 1. The dimensions of the structure such as the  $b/a$  ratio, split distance  $c$  and the boss height  $i$  are also chosen to ensure high sensitivity and linearity.

The second is the secondary sensing element which is the FBG sensing element which is fabricated using a single mode, photosensitive silica fiber (Nufern GF1) having core diameter of 9  $\mu\text{m}$  and a cladding diameter of 125  $\mu\text{m}$ , by means of phase mask technique, using Excimer KrF laser, operating at 248 nm wavelength, having an energy of around 3.0 mJ and with a variable repetition rate up-to 200Hz., resulting in the sensing element with properties and dimensions as listed in table 1. This FBG sensor element is later bonded across the centre of the split boss structure, creating a bridge between the two split bosses, completing the assembly process as shown in Fig.1c.

The developed split boss sensor was tested for 0 to 8 bar pressure range in increments of 1 bar and also benchmarked with a flat diaphragm structure of identical geometrical parameters using a dead weight hydraulic calibrator (FLUKE, Model: P3125-BAR). FBG interrogator system (Micron optics, Model SM130) with a resolution of 0.81  $\mu\text{e}$ , was used to acquire the output data.

The block diagram, photograph of the experimental setup and images of the fully assembled sensors are as shown in Figure 3(a-d).

The sensor was also subjected to dynamic pressure test, by subjecting it to a step input, Educational Instruments. The output was captured using a interrogator Make: Micron Optics, Model: Si155 which has a data acquisition rate of 5 kHz as depicted in Fig. 4(a,b).

Table 1. Parameters used in the pressure sensor design

Description	Value	Description	Value
Radius of diaphragm ( $a$ ) in mm	10	Fiber diameter of FBG ( $d_f$ ) in mm	0.125
Thickness of diaphragm ( $h$ ) in mm	0.5	Fiber length of FBG ( $l_f$ ) in mm	2
Split distance ( $c$ ) in mm	1	Fiber period of FBG ( $\Lambda$ ) in nm	530
Outer radius of the boss ( $b$ ) in mm	6	Refractive index of FBG ( $\eta_{eff}$ )	1.46
Height of the rigid mass ( $i$ ) in mm	7.5	Photoelastic coefficient ( $p_e$ )	0.22
Young's modulus steel ( $E_S$ ) in GPa	205	Young's modulus of FBG ( $E_f$ ) in GPa	72.9
Density of SS in Kg/m <sup>3</sup>	7850		
Poisson's ratio ( $\mu$ )	0.3		

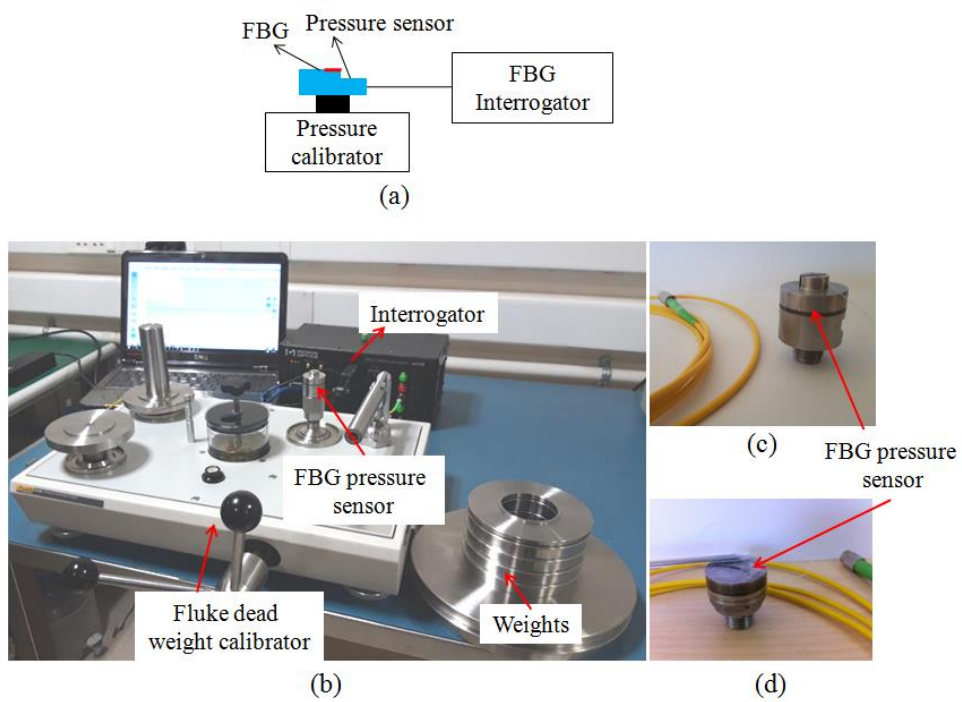


Fig. 3. (a) Block diagram; (b) Images of static calibration setup; (c) Image split boss sensor; (d) Image flat diaphragm sensor (color online)

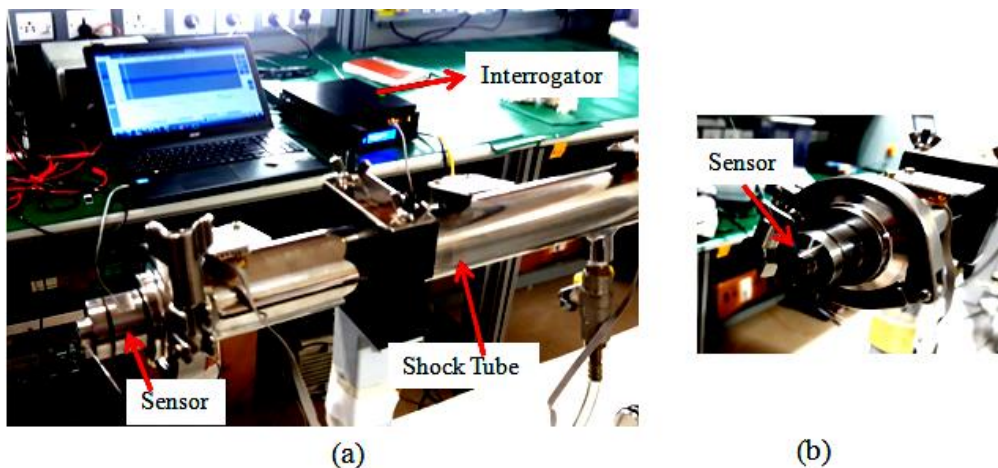


Fig. 4. Dynamic pressure calibration setup (a) Front view of the shock tube (b) Close up image of sensor on the shock tube (color online)

#### 4. Results and discussion

To check the rewards associated with the split boss design pressure sensor, the magnitudes of strain, of commonly used structures such as flat and boss diaphragm is compared with the split boss diaphragm using COMSOL Multiphysics with parameters as in Table 1.

Simulation results of the split boss structure indicate that, the strain is high along the center line of split boss diaphragm as shown in Fig. 5a. It is noticed that input pressure on the split boss diaphragm leads to widening of split boss, resulting in magnification of strain on the split boss compared to that on the diaphragm. The results indicate that the magnitude of strain is only  $\sim 30 \mu\epsilon/\text{bar}$  on the diaphragm whereas it is  $\sim 600 \mu\epsilon/\text{bar}$  on the split boss, as indicated in Fig. 5b.

The split boss structure is also compared to the other commonly available pressure sensing structures such as flat and boss diaphragms, where results indicate that the flat and boss diaphragm structures yield only  $\sim 68 \mu\epsilon/\text{bar}$  and  $\sim 45 \mu\epsilon/\text{bar}$ , making split boss structure  $\sim 10$  times

more sensitive with a linearity of 99.92%, as shown in Fig. 5c. It is evident from simulation results that the primary sensing element which is the split boss structure coupled with the methodology of bonding the secondary sensing element contributes to an increase in sensitivity of the sensor, compared to that of flat and rigid centre diaphragm structures.

Simulation studies of important geometrical dimensions of the primary sensing element such as  $b/a$  ratio, split boss distance  $c$ , and the split boss height  $i$ , which affect the performance characteristics of the primary sensing element are also optimized for maximum strain. It is seen that from Fig. 6a that the strain rapidly increases with the increase in  $b/a$  ratio, reaches its peak at 0.4 and decreases rapidly. In the case of the split distance  $c$  the strain is at its peak in the beginning and gradually decreases and later normalizes with the increase in the value of  $c$  as shown Fig. 6b. In case of boss height  $i$  the strain gradually decrease with the increase in the value of  $i$ , reaches its peak at 7mm and again decreases gradually as shown Fig. 6c.

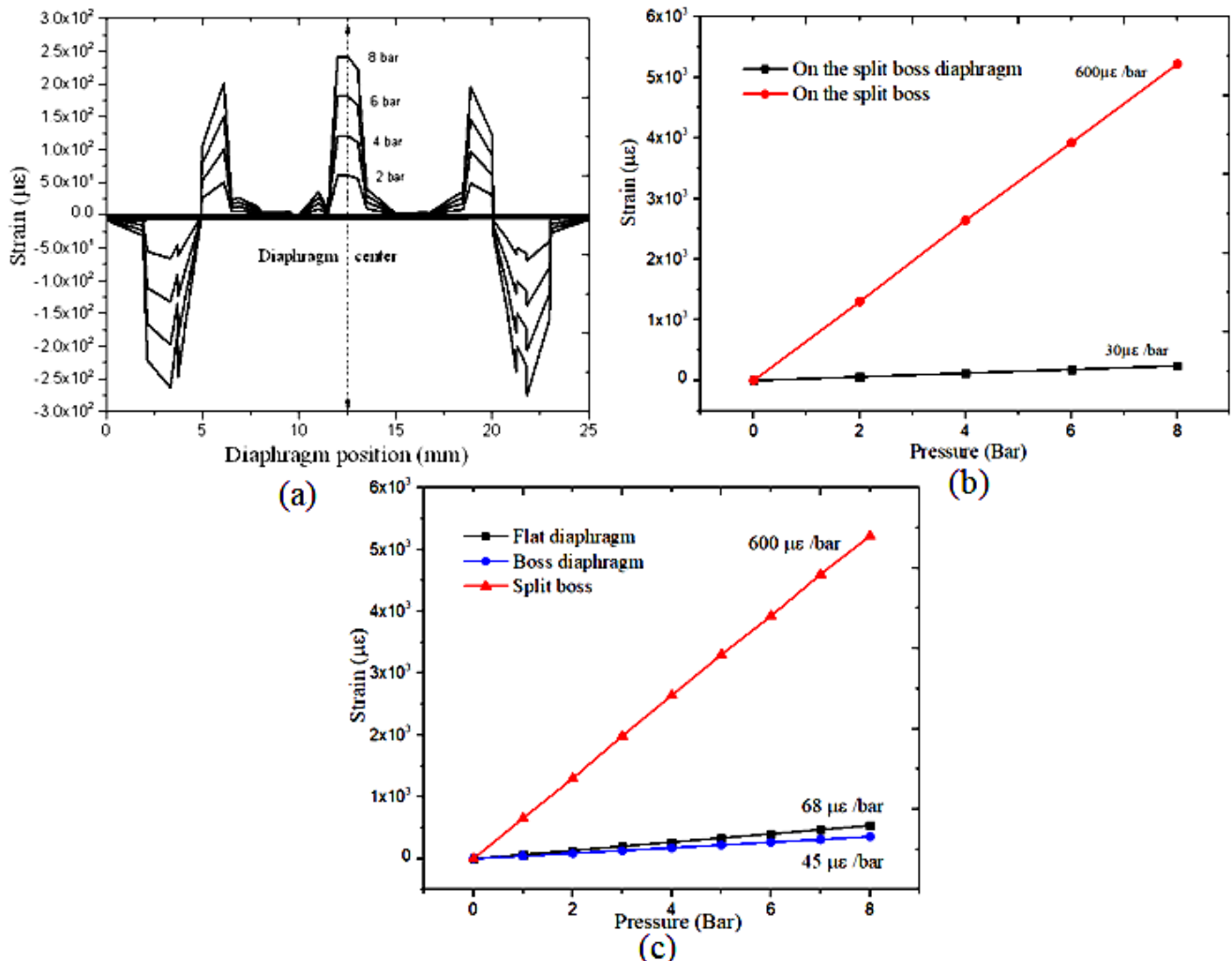


Fig. 5 Simulation studies (a) Strain distribution along the center line of split boss diaphragm (b) Comparison of strain on the split boss diaphragm and split boss (c) Comparison of strains on different types of diaphragms (color online)

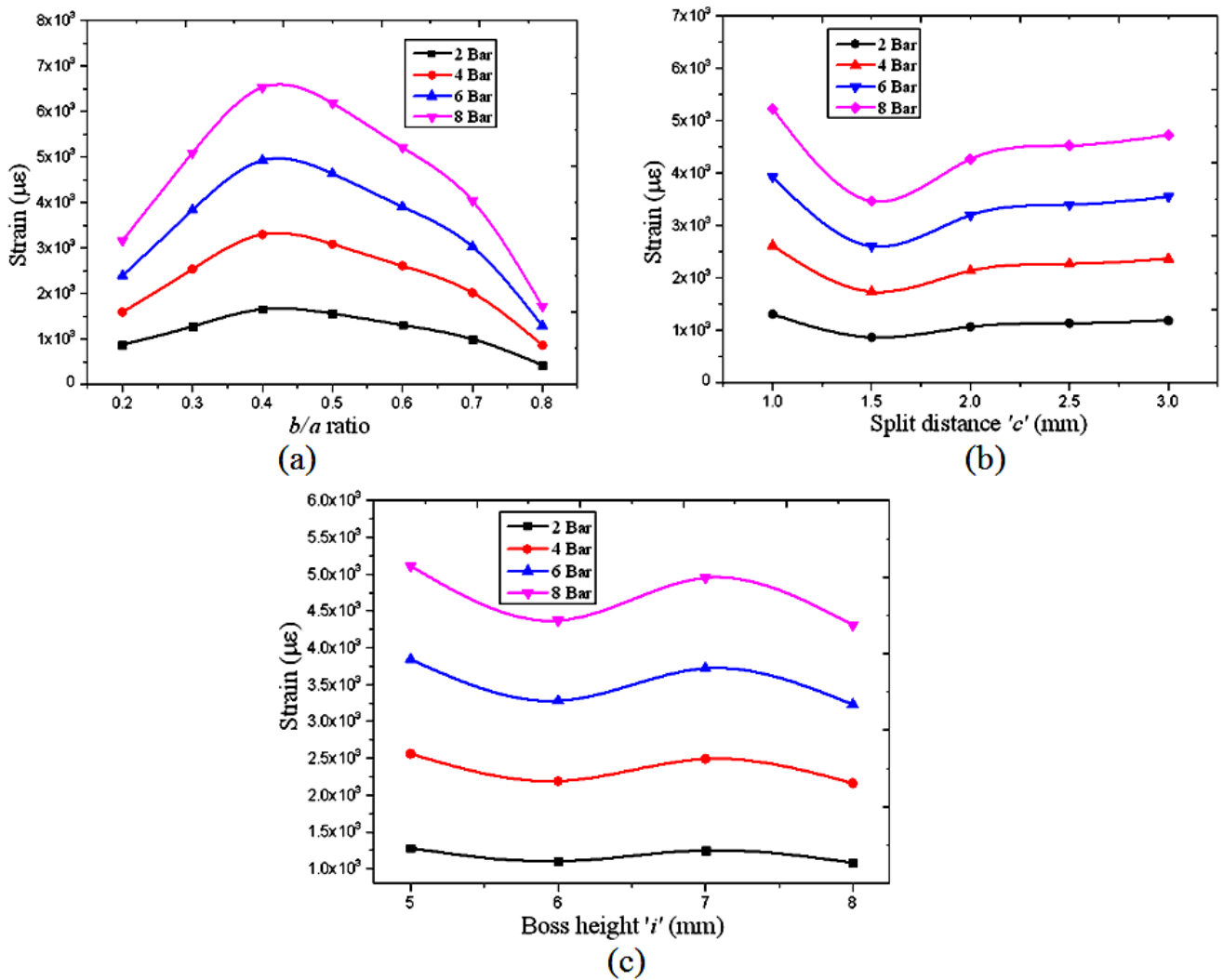


Fig. 6. Response of dimensional studies of the split boss structure with respect to the important geometrical dimensions (a)  $b/a$  ratio (b) Split distance  $c$  (c) Boss height  $i$  (color online)

Input-output static characteristics in particular sensitivity, non-linearity, hysteresis, repeatability and resolution of the pressure sensor are acquired experimentally using the system as in Fig. 3(a,b) for a pressure range of 0-8 bar in increments of 1 bar. The results of the sensor are found to be 0.742 nm/bar, 0.014 % of FSD, 0.039 % of FSD and 0.01 bar as in shown in Fig.7(a-c). The exhibited linearity was found to be 99.92 %. The sensor was also applied with three cycles of cyclic pressure and found to have good repeatability, with a

standard deviation of 0.26 as in Fig. 7b. The consistency in distribution of data also confirms repeatability, as depicted in plot Fig.7c. Strain on the fiber referenced using three methodologies namely analytical, numerical simulation and experimental displays a match with an average maximum tensile strain of  $\sim 600$   $\mu\epsilon$ /bar as shown in Fig. 8. Sensitivity of structure calculated analytically using equation (17), compared with the experimental output of the sensor are in agreement as in Fig. 9.

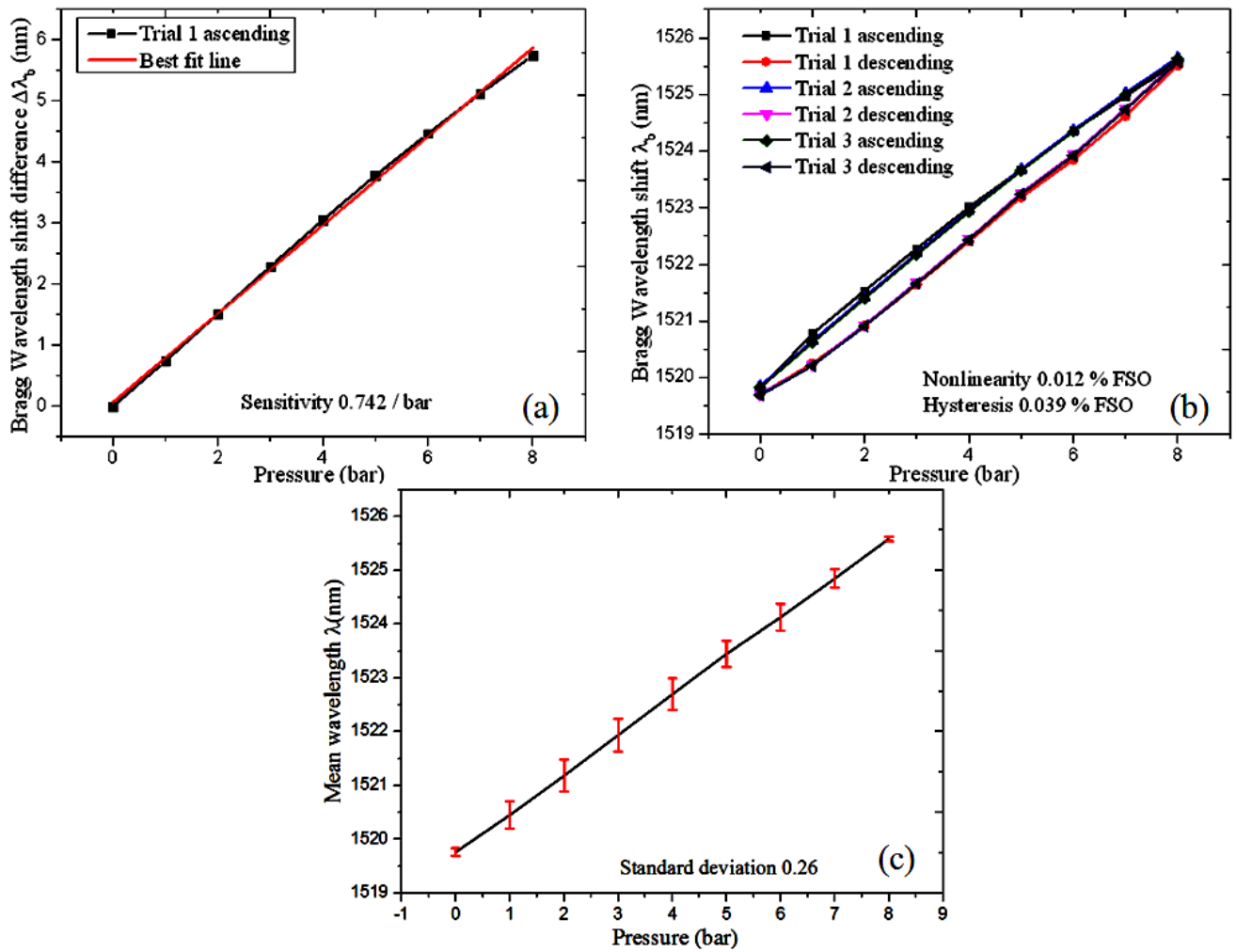


Fig. 7 Experimental results of the split boss pressure sensor (a) Sensitivity (b) Nonlinearity and Hysteresis (c) Distribution of data over mean, trials 1-3 (color online)

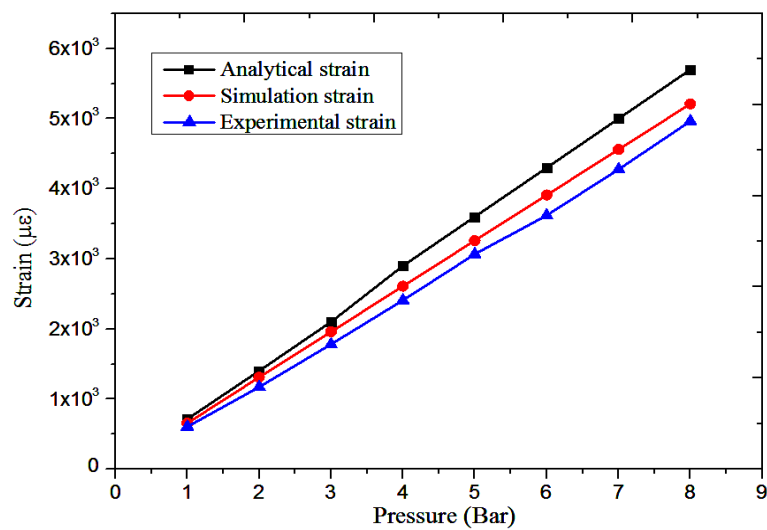


Fig. 8. Correlation of analytical, numerical simulation and experimental strain values (color online)

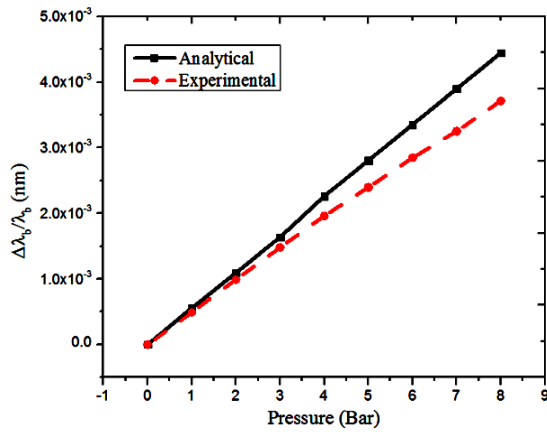


Fig. 9. Correlation of analytical and experimental results of the split boss sensor (color online)

The pressure sensitivity of the sensor is also benchmarked with a flat diaphragm FBG pressure sensor of equivalent geometrical properties, the comparison experimental study indicates that the developed sensor is ~10 times the sensitivity to that of the standard flat diaphragm FBG based sensor, as indicated in Fig. 10.

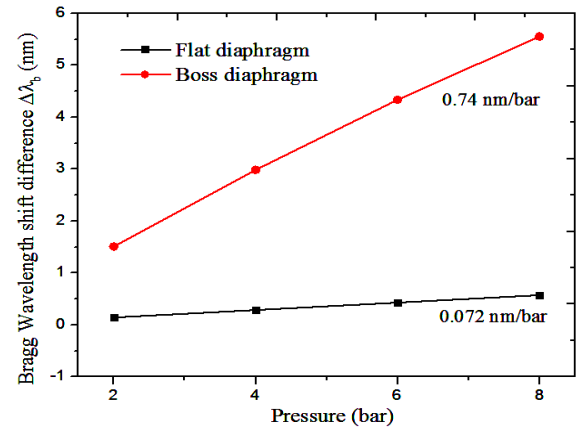


Fig. 10. Comparison of wavelength shift of split boss and flat diaphragm structures (experimental) (color online)

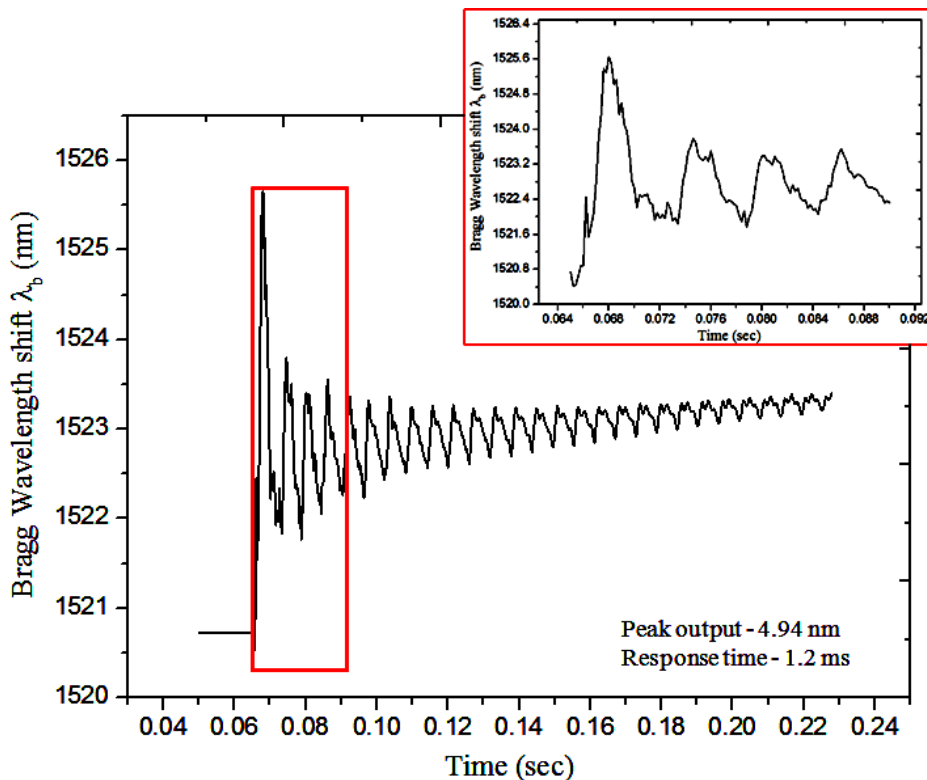


Fig. 11. Output of the sensor for dynamic pressure input with exploded view (color online)

The dynamic characteristics of the pressure sensor are acquired experimentally using an experimental setup as in Fig. 4 (a,b). The dynamic characteristics such as peak output, rise time, overshoot, settling time and damping coefficient of the sensor, for the shock tube diaphragm rupture pressure of 4.9 bar are found to be 4.94 nm, 1.2 ms, 2.95 nm, 1.99 s and 0.3 respectively as shown in Fig. 11.

The static performance of the sensor was also compared with other reported stainless steel diaphragm based FBG based pressure sensors in the literature. The developed sensor displays an improvement in sensitivity as detailed in the results shown in Fig. 12.

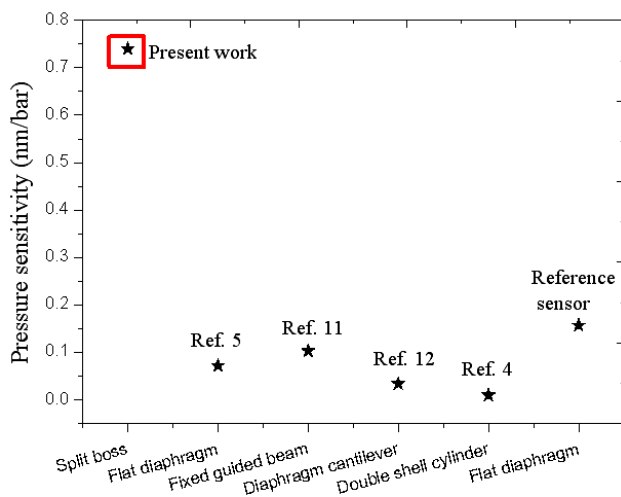


Fig. 12. Pressure sensitivity comparison of other SS diaphragm based pressure sensors from literature survey

## 5. Conclusions

A split boss based FBG pressure sensor with a SS circular diaphragm and a split boss at its centre is designed, fabricated and tested both static and dynamic pressure input. The secondary sensing element which is the FBG, is favorably bonded on either side of the split boss, resulting in a free hanging sensing structure, leading to improved sensitivity. The resulting strain on the FBG due to the input pressure is recorded to determine the applied pressure. The sensor is found to have an enhanced pressure sensitivity of 0.742 nm/bar, and also possesses good repeatability with a resolution of 0.01 bar for static pressure and for dynamic pressure the sensors vital characteristics such as peak output and rise time were 4.94 nm, 1.2 ms respectively. The static experimental test results are also in close agreement, with the developed analytical model.

## Acknowledgements

The authors express gratitude to departments of Centre for NanoScience and Engineering (CeNSE) and Instrumentation and Applied Physics (IAP), IISc, Bangalore along with Department of Instrumentation and Communication Engineering (ICE), NIT-Trichy, for providing support and facilities.

## References

- [1] Jun Huang, Zude Zhou, D. Zhang, Q. Wei, Adv. Mech. Eng. **2013**, 1 (2013).
- [2] P. Vengal Rao, K. Srimannarayana, M. Sai Shankar, P. Kishore, M. Venkata Reddy, Photonic Sensors **5**(4), 321 (2015).
- [3] Xiao Chen, Dongsheng Zhang, Mengqi Wu, Proc. AIP Conferences **1820**, 060021 (2017).
- [4] Wentao Zhang, Fang Li, Yuliang Liu, Measurement **42**, 408 (2009).
- [5] Jun Huang, Zude Zhou, Measurement **46**, 1041 (2013).
- [6] Wentao Zhang, Fang Li, Yuliang Liu, Optical Engineering **48**(2), 024402-1 (2009)
- [7] Mario Di Giovanni, Flat and Corrugated Diaphragm Design Handbook, Marcel Dekker publications, New York, 157 (1982).
- [8] Yan Sun, Ganhua Feng, George Georgiou, Edip Niver, Karen Noe, Ken Chin, Microelectronics Journal **39**, 711 (2008).
- [9] Zhongliang Yu, Yulong Zhao, Lili Li, Cun Li, Guanwu Zhou, Bian Tian, Proc. of the 9th IEEE Conference on Nano/Micro Engineered and Molecular Systems: 186 (2014).
- [10] Jian Yang, Yong Zhao, Bao-Jin Peng, Xu Wan, Sens. Act. A **118**, 254 (2005).
- [11] M. Manuvinakurake, U. Gandhi, U. Mangalanathan, M. Nayak, Optik **158**, 1063 (2018).
- [12] Min-Fu Liang, Xin-Qiu Fang, Gang Wu, Guang-Zhe Xue, Hu-Wei Li, Optik **145**, 503 (2017).
- [13] E. Vorathina, Z. M. Hafizia, A. M. Aizzuddina, K. S. Limb, Optical Fiber Technology **45**, 8 (2018).
- [14] H. Bae, M. Yu, Optics Express **20**(13), 14573 (2012).
- [15] Arnaldo Leal-Junior, Anselmo Frizzera, Camilo Díaz, Carlos Marques, Moisés Ribeiro, Maria José Pontes, Optics Express **26**(16), 20590 (2018).
- [16] V. Vinoth Kumar, A. Dasgupta, K. N. Bhat, Journal of Physics **34**, 210 (2006).
- [17] Y. Sujan, G. Uma, M. Umapathy, Sensors and Actuators A: Physical **250**, 177 (2016).
- [18] Giulio Fragiaco, Kasper Reck, Lasse Lorenzen, Erik V. Thomsen, Sensors **10**, 9541 (2010).
- [19] Raman Kashyap, Fiber Bragg Gratings, Elsevier Inc, 2nd Edition, (2010).
- [20] Abdelhak Guermata, Assia Guessouma, Nacer-Eddine Demagha, Moncef Zabouba, Zaied Bouhaf, Sens. Act A **270**, 205 (2018).
- [21] Hong-Lin Liua, Zheng-Wei Zhua, Yong Zhenga, Bang Liuc, Feng Xiaoa, Optical Fiber Technology **40**, 144 (2018).
- [22] Yi Dait, Qizhen Sun, Jianghai Wo, Xiaolei Li, Manliang Zhang, Deming Liu, Highly Sensitive Liquid-Level Sensor Based on Weak Uniform Fiber Bragg Grating with Narrow-Bandwidth, Proceedings of ICAIT 2011, (2012)
- [23] Qiang Zhaoa, Hong-Kun Zhenga, Ri-Qing Lva, Ya-Fei Gua, Yong Zhaoa, Yang Yang, Sens Act A **280**, 68 (2018).
- [24] Xinyong Dong, Xiufeng Yang, Chun-Liu Zhao, Lei Ding, P Shum, N. Q. Ngo, Smart Mater. Struct. **14**, 7 (2005).
- [25] Yanling Xiong, Jing He, Wenlong Yang, Linwen Sheng, Wei Gao, Yang Chen, Proceedings of MIC **2**, 787 (2012).
- [26] Yong Zhao, Hong-Kun Zheng, Ri-Qing Lva, Yang Yang, Sensors and Actuators A Physical **279**, 101 (2018).

- [27] S. Timoshenko, S. Woinowsky-Krieger, Theory of plates and shells, McGraw-Hill publications, New York, Symmetrical bending of circular plates, 51 (1939).
- [28] Dietmar Gross, Wolfgang Ehlers, Peter Wriggers, Jörg Schröder, Ralf Müller, Statics-Formulas and Problems, Engineering Mechanics, Springer-Verlag GmbH Germany, (2017).
- [29] Jeannot Frieden, Joël Cugnoni, John Botsis, Thomas Gmür, Dragan Coric, Composite Structures **92**, 1905 (2010).
- [30] S. H. Aref, H. Latifi, M. I. Zibaii, M. Afshari, Optics Communications **269**, 322 (2007).

---

\* Corresponding author: manjunathm@iisc.ac.in